Effects of electroconvulsive shock on the function, circuitry, and transcriptome of dentate gyrus granule neurons

Running title: Granule neuron response to electroconvulsive shock

Authors.
[1,2] Adrienne N. Santiago, PhD*
[1,2]Julia Castello-Saval, PhD*
[1,2] Phi Nguyen, PhD
[1,2] Hannah M. Chung, BS
[3] Victor M. Luna, PhD
[1,2] Rene Hen, PhD
[1,2] Wei-li Chang, MD, PhD

*asterisk indicates co-first authorship and equal contribution

Affiliations.
[1]Department of Psychiatry, Columbia University Irving Medical Center, New York, NY 10032, USA
[2]Division of Systems Neuroscience, New York State Psychiatric Institute, New York, NY 10032, USA
[3] Alzheimer's Center at Temple, Department of Neural Sciences, Lewis Katz School of Medicine, Temple University, Philadelphia, PA 19140, USA

Abstract:
Therapeutic use of electroconvulsive shock (ECS) is 75% effective for the remission of treatment-resistant depression. Like other more common forms of antidepressant treatment such as fluoxetine, ECS has been shown to increase neurogenesis in the hippocampal dentate gyrus of rodent models. Yet the question of how ECS-induced neurogenesis supports improvement of depressive symptoms remains unknown. Here, we show that ECS-induced neurogenesis is necessary to improve depressive-like behavior of mice exposed to chronic corticosterone (Cort). We then use slice electrophysiology to show that optogenetic stimulation of adult-born neurons produces a greater hyperpolarization in mature granule neurons after ECS vs Sham treatment. We identify that this hyperpolarization requires the activation of metabotropic glutamate receptor 2 (mGluR2). Consistent with this finding, we observe reduced expression of the immediate early gene cFos in the granule cell layer of ECS vs Sham subjects. We then show that mGluR2 knockdown specifically in ventral granule neurons blunts the antidepressant-like behavioral effects of ECS. Using single nucleus RNA sequencing, we reveal major transcriptomic shifts in granule neurons after treatment with ECS+Cort or fluoxetine+Cort vs Cort alone. We identify a population of immature cells which has greater representation in both ECS+Cort and fluoxetine+Cort treated samples vs Cort alone. We also find global differences in ECS- vs fluoxetine-induced transcriptomic shifts. Together, these findings highlight a critical role for immature granule cells and mGluR2 signaling in the antidepressant action of ECS.

Introduction

In the United States, 21 million adults representing 8.3% of the adult U.S. population suffer at least one major depressive episode in a single year (NIMH reports for 2021). Selective serotonin reuptake inhibitors (SSRIs) remain the first-line therapy for major depression with a response rate of ~60% and rate of ~30-40% for full remission (Al-Harbi, 2012; Rush et al., 2020). Roughly a third of patients remain treatment resistant (Zhdanava et al., 2021). Therapeutic use of electroconvulsive shock (ECS) is 75% effective for the remission of treatment-resistant depression (Husain et al., 2004). Yet the question of how ECS therapy produces these powerful effects remains unanswered.

Similar to other more common forms of antidepressant treatment such as fluoxetine (Santarelli et al., 2003), ECS has been shown to increase neurogenesis in the hippocampal dentate gyrus of rodent models. ECS promotes the activation and proliferation of quiescent neural stem cells (Segi-Nishida et al., 2008), as well as the survival and differentiation of immature adult born granule cells (iGC) (Ueno et al., 2019). Dendritic complexity, spinogenesis and axonogenesis of iGCs are all likewise

increased following ECS (Meyers et al., 2023; Schloesser et al., 2015; Zhao et al., 2012). iGCs have also been shown to be necessary for the anxiolytic effects of ECS, as pharmacogenetic deletion of iGCs blocks ECS-induced reduction of latency to feed in the novelty suppressed feeding paradigm (Schloesser et al., 2015). In human subjects, structural MRI of patients with depression reveals an increase in dentate gyrus volume after ECS treatment, as compared to volume before treatment, and the increase in dentate gyrus volume correlated with symptom improvement (Nuninga et al., 2020). Interestingly, volume increase was observed in the DG but not the CA1 or CA3 regions of the hippocampus. While we cannot attribute volumetric changes solely to the bodies and neuropil of adult-born cells, this finding does highlight the importance of DG neuroplasticity in ECS response. Further supporting the role of iGCs, postmortem tissue from patients treated with ECS exhibit greater levels of proteins expressed by immature neurons, including doublecortin (DCX) and STMN1 (Loef et al., 2023). Yet the question of how ECS-induced neurogenesis supports improvement of depressive symptoms remains unknown.

Several properties of iGCs distinguish them from the more mature granule cells (mGCs) and provide insight as to their unique role in the DG network. Our group (Danielson et al., 2016; Drew et al., 2016) and others (Li et al., 2024; McHugh et al., 2022) have shown that iGCs are more active than mGCs, yet paradoxically contribute to overall DG inhibition and maintenance of a sparse network activity which may be necessary for optimal execution of DG dependent behaviors (McHugh et al., 2022). iGCs indirectly suppress mGC activity via inhibitory interneurons (Danielson et al., 2016) and directly suppress mGCs via post-synaptic metabotropic glutamate receptor 2 (mGluR2)-mediated activation of G protein coupled inwardly rectifying potassium channels (Luna et al., 2019). To date, there have not yet been any publications to explore the role of mGluR2 in ECS. Interestingly, systemic application of both mGluR2/3 agonists (Linden et al., 2004; Munguba et al., 2024) and antagonists (Yoshimizu et al., 2006) are associated with anxiolytic effects in mice. This is likely due to the heterogenous actions of mGluR2 in different brain regions. Delivery of systemic mGluR2 agonist also reduces expression of the immediate early gene cFos in the dentate gyrus (Linden et al., 2004). Here, we ask whether ECS likewise reduces mGC activity and whether the behavioral effects of ECS require mGluR2.

Recent technological advances in RNA sequencing (RNAseq) allow us to profile transcriptomic changes in a cell-type specific manner. The question of how ECS shifts gene expression in individual granule cells is currently unknown. Single nucleus RNAseq has been used to profile neuroblasts, iGCs, and mGCs throughout development and into adulthood (Hochgerner et al., 2018). Bulk-RNAseq of the adult

hippocampus has shown that chronic ECS broadly increases expression of genes associated with neurogenesis, including Sox11 (Rimmerman et al., 2022), yet direct conclusions about ECS-induced transcriptomic shift in granule neurons themselves could not be drawn from that study. Our study profiles granule neurons after chronic ECS administration, when behavioral antidepressant-like effects of ECS are observed.

Methods.

Mice.

All procedures were conducted in accordance with the U.S. NIH Guide for the Care and Use of Laboratory Animals and the Institutional Animal Care and Use Committees of New York State Psychiatric Institute and Columbia University. Adult male mice were housed in a vivarium grouped 2-4 mice/cage, maintained on a 12-hour light cycle. For figures 1-3,5-6 mice began experimental procedures at 10 weeks of age. For figure 4, mice began experimental procedures at 17-45 weeks, with no between-group differences in age (one-way ANOVA: $F(3, 20) = 0.2933$, $P=0.8297$). C57/6J mice were obtained from Jackson Laboratory. Transgenic mice were bred on a C57/6J background and bred in house. Both Nestin-CreER^{T2} (Fig 3)(Dranovsky et al., 2011) and Dock10-Cre (Fig 4)(Kohara et al., 2014) transgenic mice were used.

ECS.

Mice were briefly anesthetized with 2% isoflurane, delivered through a nose cone at an oxygen flow rate of 1 L/min. Electroshocks were delivered to anesthetized mice through ear clipped electrodes at 120 Hz and 50 mA, for a duration of 1 second (Fig 1b). Ringers salt solution was applied to the ear prior to shock to improve conductance. Mice received ECS treatment once every other day for a total of 10 sessions (20 days). Sham mice received isoflurane anesthesia and application of Ringers solution and ear clips, with no delivery of electroshock current.

Drug administration.

As in previous publications (David et al., 2009; Dieterich et al., 2019), Cort (Sigma) was dissolved in .45% betacyclodextrin (vehicle) and delivered via drinking water in opaque bottles replaced every 3-4 days. Mice received 35 ug/ml of Cort, equivalent to 5mg/kg/day. Due to sex differences in response to chronic Cort stress (Bertholomey et al., 2022), we limited this study to male mice.

Focal X-irradiation.

Hippocampal irradiation was conducted as previously described (Sahay et al., 2011). After anesthesia with 6 mg/kg sodium pentobarbital i.p., 10-week-old mice were

placed in a stereotaxic frame and covered by a lead shield with a 3.22 x 11-mm window positioned to allow focal application of X-irradiation to the hippocampus. X-rays were filtered using a 2 mm Al filter, the corrected dose rate was approximately 1.8 Gy per min and the source to skin distance was 30 cm. A cumulative dose of 5 Gy was given over the course of 2 minutes and 47 seconds over 3 days, with 3 days between each X-ray session. Control mice did not receive radiation, but were anesthetized with irradiated mice throughout the experiment.

Virus.
The shRNA vector Ef1a-DIO-U6-mGluR2-shRNA was a generous gift from Marcus Meinhardt that we had packaged by VectorBuilder into an AAV8 vector. AAV8-cmv-DIO-GFP was used as a control (VectorBuilder).

Surgery.
Surgery for bilateral ventral DG virus injection was performed as described previously (Anacker et al., 2018). Briefly, mice were anesthetized with 1.5% isoflurane at an oxygen flow rate of 1 L/min, and head-fixed in a stereotactic frame (Kopf Instruments, Tujunga, CA). Eyes were lubricated with an ophthalmic ointment, and body temperature maintained at 37°C with a warm water recirculator (Stryker, Kalamazoo, MI). The fur was shaved and incision site sterilized prior to beginning surgical procedures, and subcutaneous saline and carprofen were provided peri-operatively and for 3 days post-operatively to prevent dehydration and for analgesia.

Behavior.
Novelty-suppressed feeding (NSF) was performed as previously described (Samuels and Hen 2011). Briefly, mice are food deprived for 16 hrs before placement in a brightly-lit arena with a food pellet taped to the center of the arena. This provides a conflict anxiety test whereby the motivation to eat competes with the risk to enter the center of a brightly lit arena. Forced-swim test was performed as previously described (Hill et al., 2015). Briefly, 3L beakers were filled with 2500 ml of tap water at 25C. Time spent actively swimming vs passively floating was recorded using Videotrack software (ViewPoint Behavior Technologies).

Electrophysiology. We performed whole-cell current clamp recordings on GCs while optogenetically manipulating immature iGCs as previously described (Luna et al., 2019).

IHC. For histology, mice were transcardially perfused with 4% paraformaldehyde (PFA; EMS) in 1X phosphate buffer solution (PBS), after which brains were removed and post-

fixed in 4% PFA for 24 h. They were transferred to a 30% sucrose solution in 1X PBS for 2 days, after which they were flash-frozen in methylbutane and coronally sliced on a cryostat (Leica CM 3050S) at a thickness of 40 μm. Immunohistochemistry for DCX and cFos were performed as previously described (Drew et al., 2016). Briefly, for DCX, antigen retrieval was performed with heat treatment to 80C in pH8 citrate buffer. Tissue was then incubated in blocking buffer containing 10% normal donkey serum and 0.2% triton for 1 hr. Primary antibody (Cell Signaling Tech #46042S) was diluted 1:400 and incubated with tissue overnight at 4C. After washing 3X in PBS, Alexa Fluor donkey anti-rabbit 488 secondary antibody was used. For cFos, (Cell Signaling Tech #2250), antibody was diluted 1:400 and no antigen retrieval step was applied. All slides were imaged on a Leica SP8 and all IHC images were analyzed with ImageJ software (NIH).

RNAscope.

RNAscope (ACDBio) for GRM2 was performed according to manufacturer instructions to confirm shRNA knockdown in virally transfected granule neurons.

Flow cytometry for RNAseq.

Animals were perfused transcardially with ice-cold 1X PBS and hippocampi were isolated under a dissecting microscope where meninges and excess myelin were removed. For sorting neuronal nuclei for downstream RNA-sequencing, cells were isolated as described (Nguyen et al., 2020). Briefly, hippocampi were mechanically dissociated using a glass tissue homogenizer in isolation medium (HBSS, 15 mM HEPES, 0.6% glucose, 1 mM EDTA pH 8.0). Cells were filtered and then pelleted at 300 g for 5 minutes at 4°C before being resuspended in 22% Percoll (GE Healthcare) and centrifuged at 900 g for 20 minutes with acceleration set to 4 and deceleration set to 1 in order to remove cellular debris. Pelleted nuclei were then washed with isolation medium and incubated in block solution consisting of 1% BSA (Sigma-Aldrich, A2153). Alexa Fluor 488 mouse anti-NeuN (1:1500; Millipore, MAB377X) and DAPI (Sigma-Aldrich, D9542) were used to detect neuronal nuclei. Cell multiplexing oligos (10x Genomics, 3' CellPlex Kit Set A, 1000261) were incubated with each sample for 5 min at room temperature following washes of primary antibody stain. Gating was based on fluorescence minus one (FMO) negative staining controls. All data analysis was performed using FlowJo™ software. Cells were sorted on a Sony MA900 cell sorter at the Columbia Stem Cell Initiative Flow Cytometry core facility at Columbia University Irving Medical Center. Neuronal nuclei were gated based on forward/side scatter, DAPI+, and NeuN+.

Single nuclei RNA-sequencing.

FACS purified neuronal nuclei were sequenced using the 10 Genomics Single Cell Gene Expression 3' platform (v3). Nuclei barcoded with cell multiplexing oligos were pooled into 4 samples with each sample containing nuclei from one mouse from each condition (Vehicle, Cort, Fluoxetine + Cort, ECS + Cort). Approximately 15,000 nuclei were loaded into each well of Chromium Chip A according to the manufacturer instructions and combined into droplets with barcoded beads using the Chromium controller. Libraries were prepared by the JP Sulzberger Columbia Genome Center following the instructions in the Chromium Single Cell 3' Reagent Kits version 3 user guide. The samples were sequenced to an average depth of 40,000-60,000 reads on an Illumina Novaseq 6000 sequencer.

Single nuclei RNAseq data analysis.

Sequenced samples were processed by the JP Sulzberger Columbia Genome Center using the Cell Ranger 7.01 pipeline and aligned to the mm10-2020-A mouse reference transcriptome. Clustering and differential expression analysis were conducted using Seurat version 4 (Butler et al., 2018; Satija et al., 2015). Cells with fewer than 500 detected genes/cell or over 3000 genes/cell, comprising the lower and upper 5% of cells respectively, or more than 5% mitochondrial RNA were excluded during quality control steps before identification of variable genes in the dataset, cell centering, and scaling. Additionally, 3000 genes were eliminated that were expressed by fewer than 5 cells in the dataset. The "SCTransform" function in Seurat was used for normalization and variance stabilization of molecular count data. Approximately 3000 of the most variable genes were identified and used for calculating nearest neighbors, PCA, and UMAP plots. 50 principal components were calculated using these genes and the first 30 PCs were used for subsequent calculations. Clustering and UMAP plots were computed using Seurat (Butler et al., 2018; Satija et al., 2015).

Gene lists for mature or immature neuronal profiles were derived from Hochgerner et al., 2018. The "AddModuleScore" function in Seurat was used to generate module scores of mature and immature neuronal profiles. Differentially expressed genes were identified using the "FindMarkers" function in Seurat. Only genes expressed in 25% of the cells in a given condition and a minimal log fold change threshold of 0.25 were included in the differentially expressed gene list. GO analysis was conducted using the Metascape webpage (https://www.metascape.org).

Statistical analysis.

All statistical analyses were preformed using Prism (GraphPad). Generally, normally distributed data were analyzed by two-way ANOVA to assess ECS effects alongside experimental manipulations ie x-irradiation and mGluR2 downregulation. Because NSF recordings are capped at 400s, we frequently observed ceiling effects in measurements

of latency to feed, producing non-parametric data. We therefore used the Kruskal-Wallis test to compare medians across groups with post-hoc Dunn's test corrected for multiple comparisons. We also report a survival curve for latency to feed which we analyzed with the standard Mantel-Cox test.

Results.

Mouse model of ECS.

10 week-old C57/Bl6 mice were treated with vehicle or 5mg/kg corticosterone (Cort) in drinking water to maintain a stress-like state throughout the experiment, (protocol as published (David et al., 2009); Fig 1a). After 4 weeks, mice from Vehicle and Cort groups received 10X ECS or Sham treatment. To induce ECS, electroshocks were delivered to anesthetized mice through ear clipped electrodes at 120 Hz and 50 mA, for a duration of 1 second (Fig 1b). This current-induced tonic/clonic seizures, identifiable by acute arching of the back followed by rhythmic movement of limbs and sustained tension in the tail. Because repeated ECS is more effective than a single dose and more accurately mimics designs for treatment in humans (Henningsen et al., 2013; Ittasakul et al., 2020; Suzuki & Masuda, 1999), we repeated ECS on alternate days for 10 sessions. Sham mice received anesthesia and placement of ear clips, but no administration of electroshock. Duration of seizure was unaffected by Cort vs vehicle administration (two-way ANOVA; $F(1,9) = 0.07$; $p = 0.79$; Fig S1a).

We first established replication of published behavioral effects of ECS on anxiety-like and depression-like behaviors (Schloesser et al., 2015; Suzuki & Masuda, 1999). During acclimation to behavioral testing, locomotion was observed in a simple arena for 10 min. Total locomotion did not differ significantly between groups (one-way ANOVA: $F(3, 35) = 1.378$; $p=.2655$; Fig S1b). For the novelty suppressed feeding test (NSF), mice were deprived of food for 24 hrs before they were given access to a food pellet in the center of a novel arena. Latency to consume food is recorded, before the test is repeated in the home cage. Latency to approach food in the novel arena vs the home cage is an established indicator of anxiety-like behavior (Samuels & Hen, 2011; Santarelli et al., 2003). In the novel arena, ECS-treated mice exhibit a decreased latency to feed in the Cort group (adjusted $p= 0.0365$) that is absent in the vehicle group ($p = 0.9999$; Fig 1c; Kruskal-Wallis test for nonparametric distributions ($p = 0.0017$) with post-hoc Dunn's test). A significant difference in latency to feed between groups was likewise confirmed by survival curve (Mantel-Cox: $p = .0003$). By contrast, ECS had no effect on latency to feed observed within the home cage (two-way ANOVA $F(1, 34) = 0.02409$; $p = 0.8776$). In the Forced Swim Test (FST), ECS mice spent less

time immobile vs Sham in both the Cort ($p = .0107$) and Vehicle ($p = .0052$) treated groups (two-way ANOVA: $F(1, 35) = 19.31$; $p < .0001$; Sidak's test post hoc; Fig 1d). Together, these findings support previous publications establishing the anxiolytic and antidepressant effects of repeated ECS, particularly after exposure to chronic stress (Schloesser et al., 2015; Suzuki & Masuda, 1999).

Effects of ECS on iGCs.

A subset of 5 mice per group were analyzed for expression of doublecortin (DCX), which is expressed in the dendrites and soma of immature adult-born granule neurons (Fig 1e). Estimating the relative density of DCX expression in the granule cell layer averaged over the full dorsoventral axis of the DG, we found that ECS treated mice had more DCX expression vs Sham mice, regardless of Cort ($p = .0045$) vs Vehicle ($p = .0005$) treatment (Fig 1f; two-way ANOVA: $F(1, 16) = 34.57$; $p < .0001$; Sidak's test post hoc). When we limited our analysis to the dorsal DG, we likewise found that ECS treated mice expressed higher density of DCX vs Sham in both Cort ($p=.0185$) and vehicle treated mice ($p = .0008$; two-way ANOVA: $F(1, 16) = 27.56$; $p < .0001$; Sidak's test post hoc). When we limited our analysis to the ventral DG, we again found that ECS treated mice expressed higher density of DCX vs Sham in both Cort ($p=.0084$) and vehicle treated mice ($p = .0080$; two-way ANOVA: $F(1, 16) = 22.38$; Sidak's test post hoc). These findings are in keeping with past publications that have reported increased neurogenesis after ECS as well as longer and more complex dendritic branches in DCX immunoreactive dendrites (Meyers et al., 2023; Ueno et al., 2019).

Effects of x-irradiation to ablate DG neurogenesis on ECS efficacy.

To assess the role of iGCs in mediating the effects of ECS, we performed focal DG X-irradiation (X-IR) vs Sham (X-sham) followed by ECS vs Sham (E-sham) in Cort treated mice (Fig 2a). X-IR eliminated expression of DCX as has been shown previously (Luna et al., 2019; Tuncdemir et al., 2023)(Fig 2b).

In the NSF test, we observed that ECS treated mice had a higher latency to eat after X-IR vs ECS/X-sham mice (adjusted $p = 0.0050$; Fig 2c; Kruskal-Wallis test for nonparametric distributions (adjusted $p = 0.0030$) with post-hoc Dunn's test). By contrast, X-IR had no significant impact on latency to eat within the home cage for either ECS ($p = .3500$) or E-sham groups ($p = .254$). A significant between-group difference in latency to feed in the novel arena was likewise confirmed by survival curve (Mantel-Cox: $p = .0015$).

In the FST, ECS mice were immobile for significantly less time in the X-sham group vs X-IR treated mice ($p = 0.0155$, two-way ANOVA interaction effect: $F(1, 34) = 6.135$; $p < .0184$; Sidak's test post hoc; Fig 2d). Within the X-sham group, ECS mice spent less time immobile vs E-sham mice ($p = .0107$). Together, these findings support a critical role for iGCs in mediating ECS-induced improvement of both anxiety-like and depressive-like behaviors.

mGluR2 mediates iGC-driven inhibition in mGCs after 10x ECS.

Several studies from our group (Anacker et al., 2018; Danielson et al., 2016) and others (Li et al., 2024; McHugh et al., 2022) have suggested that iGC support DG function by decreasing activity in more mature cells. To assess whether DG activity was generally sparser after ECS vs Sham, we quantified expression of the immediate early gene, cFos, after exposure to home cage (Fig 3a). We found that cFos expression was lower in ECS vs Sham treated mice (Student's T test; $p = .0007$; Fig 3b).

In addition to inhibitory cell recruitment, iGCs are capable of directly inhibiting mGCs via mGluR2-mediated postsynaptic hyperpolarization (Luna et al., 2019). To determine whether this type of inhibition was enhanced by ECS vs Sham in subjects maintained on Cort, we used whole-cell current clamp recordings in DG brain slices (Fig 3c). For these experiments, we crossed a Nestin-CreER^{T2} mouse line with a floxed channelrhodopsin-EYFP (ChR2-EYFP) expressing mouse line, which enabled us to induce expression of channelrhodopsin-EYFP in iGCs conditionally upon delivery of tamoxifen (Fig 3D). We optogenetically stimulated 0-6 week-old iGCs and recorded synaptic responses in the presence of AMPA-, NMDA-, and GABAA-receptor antagonists (Luna et al., 2019) (Fig 3e). We observed a significantly larger inhibitory response in mGCs of ECS-treated mice than Sham controls (Fig 3f; Sham=-0.12±0.04 mV, N=4; ECS=0.25±0.02, N=6; Student T-test, $p = .0162$). The inhibitory currents were blocked with bath application of the mGluR2/3 antagonist, APICA, indicating that mGluR2 mediated the postsynaptic inhibitory signal (Luna et al., 2019). Together these findings suggest that iGC activation may contribute to the sparsity of the granule cell network by engaging mGluR2 present on mGCs.

Behavioral effects of ECS are blunted by mGluR2 knockdown in ventral DG.

To test whether mGluR2 expression in mGCs is necessary for the behavioral effects of ECS, we selectively knocked down mGluR2 expression in ventral DG granule neurons (Fig 4a). The ventral DG was targeted specifically because this subregion is known to play a greater role in anxiety-like and depressive like behavior (Kheirbek et al., 2013), and silencing mGCs in the ventral DG has been shown to support resilience to chronic

stress (Anacker et al., 2018). Cre-dependent viruses AAV8-shRNA-mGluR2 or AAV8-GFP control were delivered to the ventral hippocampus of Dock10-Cre mice so that viral transcription was limited to ventral DG granule neurons. A week following surgery, mice began Cort treatment in drinking water. After 4 weeks, mice receive 10x ECS or Sham, followed by behavioral testing. We confirmed that the shRNA-mGluR2 virus did in fact reduce expression of mGluR2 RNA specifically in the ventral DG via RNAscope in situ hybridization (Fig 4b).

In the NSF test, among control subjects, latency to eat in the novel arena was reduced in ECS mice vs Sham ($p = 0.0408$; Fig 4c; Kruskal-Wallis test for nonparametric distributions ($p = 0.0072$) with post-hoc Dunn's test). By contrast, no effect was observed between ECS and Sham mice that had received mGluR2-shRNA ($p = .4319$). A significant between-group difference in latency to feed in the novel arena was likewise confirmed by survival curve (Mantel-Cox: $p = .0012$). In the home cage, no effect of ECS or mGluR2 knockdown on latency to eat was observed (two-way ANOVA; ECS: $F(1, 34) = 0.02409$, $p = .3335$; mGluR2-shRNA: $F(1, 34) = 0.3458$, $p = .5604$; interaction: $F(1, 34) = 0.9624$, $p = .3335$). In the FST, we observed a trend towards an ECS effect on time spent immobile (two-way ANOVA; ECS: $F(1, 21) = 3.139$, $p = .0909$; post-hoc Sidak's test: for ECS effect in AAV-GFP group: $p= 0.1809$; for ECS effect in AAV-mGluR2-shRNA: $p = .7173$).

To assess whether ECS-induced DG network sparsity was likewise blunted by mGluR2 knockdown, we quantified cFos expression after exposure to home cage (Fig 4e). We found that among control virus subjects, cFos expression was reduced in ECS mice vs Sham ($p = .0280$; two-way ANOVA with post-hoc Sidak's test: ECS effect: $F(1, 17) = 7.389$, $p = .0146$). By contrast, no effect was observed between ECS and Sham mice that had received mGluR2-shRNA ($p = .5066$), suggesting that mGluR2 may be necessary for ECS-induced suppression of mGC activity. Together, these findings suggest that mGluR2 is necessary for ECS-induced resilience to chronic stress.

Both ECS and Fluoxetine drive transcriptomic shifts indicating greater neuroplasticity and more prominent immature phenotype among granule neurons. To characterize granule neuron response to antidepressant treatment, we performed single nucleus RNA sequencing on dissected hippocampi from four treatment groups: vehicle (Veh), Cort, Cort plus fluoxetine (Flx), and Cort plus 10x ECS (N=3 per group; Fig 5a). Neuronal nuclei were isolated using fluorescent activated cell sorting (FACS) for NeuN+ nuclei. Transcriptomic profiles of hippocampal neuronal nuclei were generated and granule cells were identified by expression of *Prox1*, *Dock10*, and *Stxbp6* (N=8,318 nuclei). Distinct cell states for Veh, Cort, Flx, and ECS groups

emerged, indicating that granule neurons of each group are transcriptomically distinct (Fig 5b).

To further investigate the role of immature cells in antidepressant treatment, we used differentially expressed genes (DEGs) identified by Hochgerner et al 2018 as characteristic of immature vs mature cells to create module scores of a mature vs immature phenotype (Fig 5c). We found that, in our sample, mature vs immature phenotype cells produced distinct clusters (Fig 5d). Interestingly, the percent of neurons in the immature phenotype cluster differed by treatment group (Fig 5e; one-way ANOVA, $F(3, 8) = 11.00$, $p = .0044$). Post hoc Tukey's tests revealed that both Flx ($p = .0152$) and ECS groups ($p = .0083$) had a significantly greater proportion of immature-clustered granule cells vs Cort.

Both ECS and Flx exhibited upregulation (vs Cort) of key genes known to play a critical role in neurodevelopment and neuroplasticity (see supplemental table 1 for a full list of DEGs for ECS vs Cort and Flx vs Cort). These include Neuregulin 1 and 3 (Nrg1, Nrg3), Neurexin 3 (Nrxn3), and Ncam2. ECS also upregulates Nrxn1, while Flx upregulates both BDNF and the gene encoding TrkB (Ntrk2). Both ECS and Flx also exhibit downregulation of genes associated with mature granule cell identity (Kobayashi et al., 2010), including Calb1, Dock10, and Rbfox3.

Despite the above similarities, and consistent with the UMAP projection (Fig 5b), we also find strong differences in Flx- and ECS-induced transcriptomic shifts. While Flx induces upregulation of 1125 DEGs and downregulation of 645 DEGs, ECS upregulates only 209 DEGs and downregulates 1560 DEGs (Fig 6a,b). Flx also induces a stronger transcriptomic response, with greater average fold change and -LogP value for DEGs (Fig 6c,d). Thus, ECS achieves equivalent behavioral antidepressant effects vs Flx while unexpectedly inducing a more modest transcriptomic shift.

Discussion.

Summary of results.

Here, we demonstrated that chronic ECS-induced anxiolytic and antidepressant-like effects require iGCs. We showed for the first time that ECS-induced behavioral effects are blunted by downregulation of ventral granule neuron mGluR2, and also that electrophysiological effects of ECS are reversed with mGluR2 antagonism. We then used single nucleus RNAseq to characterize the transcriptomic shift induced by ECS or Flx vs Cort alone. We show that ECS and Flx both induce a shift towards greater expression of an immature vs mature granule neuron profile, but that the overall expression patterns of the two interventions is distinct.

iGCs and the sparse DG.
In this report, our behavioral, histochemical, electrophysiological, and transcriptomic data converge in their support of the hypothesis that iGCs play a critical role in the antidepressant action of ECS. While several publications have detailed the neurogenic effects of ECS (Segi-Nishida et al., 2008; Ueno et al., 2019), this is the first publication to demonstrate that ECS facilitates iGC-driven inhibition of mature granule neurons. We show here that chronic ECS reduces DG cFos expression over a week after seizure cessation. This finding provides a sharp contrast to the acute effect of ECS, which is known to upregulate activity-dependent genes like cFos post seizure (Daval et al., 1989). We hypothesize that iGC-induced suppression of mature GNs contributes to the sparse DG network activity that has been shown to support stress-resilience (Anacker et al., 2018).

Role of mGluR2.
To date, this is the first study of the role of mGluR2 in ECS-induced behavior. Our past work has shown that iGCs can directly inhibit mGCs via mGluR2-mediated activation of G protein-coupled inwardly rectifying potassium currents (GIRKs)(Luna et al., 2019). mGluR2 is expressed on both axon terminals and proximal dendrites of granule cells (Brunner et al., 2013). While axon terminal mGluR2 has been shown to limit mGC firing via modulation of calcium conductance, dendritic mGC mGluR2 expression has been shown to engage GIRKs (Brunner et al., 2013). Interestingly, both mGluR2 and GIRK expression is absent in very immature granule cells and increases expression with maturity (Gonzalez et al., 2018; Ma et al., 2023). This suggests that postsynaptic inhibitory effects of mGluR2 are specific to the more mature mGC population. We did not observe an increase in Grm2 expression following ECS, and in fact observed a decrease in a small percentage of cells. This could be related to the decrease of maturation-related genes in the ECS sample. Additionally, any analysis limited to RNA vs protein will not be able to resolve the balance between expression of mGluR2 dimers vs monomers, which is an important distinction considering that only mGluR2 dimers are capable of evoking synaptic signals.

ECS and Flx increase of transcription factors associated with neuroplasticity and immaturity.
We show here that both Flx and ECS increase transcription of several genes known to play a critical role in iGC survival, growth, and migration, including the neurexins, neuregulins, and Ncam highlighted in this work. We then used the Hochgerner 2018 study to profile granule neurons as having a more immature vs mature phenotype, and found a greater number of immature-phenotype cells in the Flx and ECS populations vs

Cort. This finding parallels work using BrDU and DCX labeling, in situ hybridization, and neuronal tracing to show that both Flx (David et al., 2009) and ECS (Segi-Nishida et al., 2008; Ueno et al., 2019) promote the survival, growth, and dendritic arborization of confirmed adult-born iGCs. ECS may additionally lengthen the amount of time adult-born cells retain their immature phenotype, as ECS has also been shown to suppress mature marker expression during the late maturation stage of neurogenesis (Ueno et al., 2019). Unlike in those studies, we did not use any label-retention marker, such as BrDU, to time stamp iGCs in this study. Therefore, we cannot positively identify cells with an immature profile as adult-born iGCs. There remains the possibility that, in addition to stimulating neurogenesis, ECS and Flx also induce an immature-phenotype among embryonically born granule cells or adult-born granule cells that are well outside the 4-8 week window commonly associated with immaturity. In fact, there is evidence to suggest that Flx is capable of inducing an immature phenotype among mGCs (Hagihara et al., 2019). This phenomenon may likewise occur following ECS. Therefore, ECS may have a dual function in the DG by supporting both the development of iGCs as well as the dematuration of mGCs. This may be why we observe that immature and mature populations are quite distinct in Cort and Veh UMAP clusters, but are bridged in Flx and ECS UMAP clusters, indicating greater ambiguity between iGC and mGC clusters. This suggests that antidepressant treatment supports a greater number of cells in the transitional space between immature and mature phenotype clusters, which could be attributed both to slower maturation of iGCs as well as dematuration of mGCs.

Conclusions.

Overall, these findings provide insight into the neurobiological mechanisms possibly underlying the therapeutic effects of ECS. We found that ECS-induced stress resilience requires both iGCs and mGluR2 expression in ventral mGCs. The involvement of mGluR2 in mediating the effects of ECT on behavior highlights a specific molecular pathway that could be targeted for the development of novel therapeutic interventions for mood disorders. Modulating mGluR2 activity or expression may offer new avenues for enhancing the efficacy of ECS or developing alternative treatments with similar mechanisms of action.

This study is the first to examine the effects of chronic ECS on the granule neuron transcriptome. We found that ECS and Flx both induce a transcriptomic shift towards a more immature phenotype in granule neurons, suggesting a potential mechanism underlying their therapeutic effects. However, while both treatments induce similar behavioral effects, they elicit distinct transcriptomic changes in mature neurons of the DG, suggesting that the different treatments may additionally engage unique

neurobiological mechanisms and modes of action. The distinct transcriptomic changes induced by ECS compared to Flx underscore the complexity of mood regulation and the diverse pathways through which antidepressant effects can be achieved.

Figures.

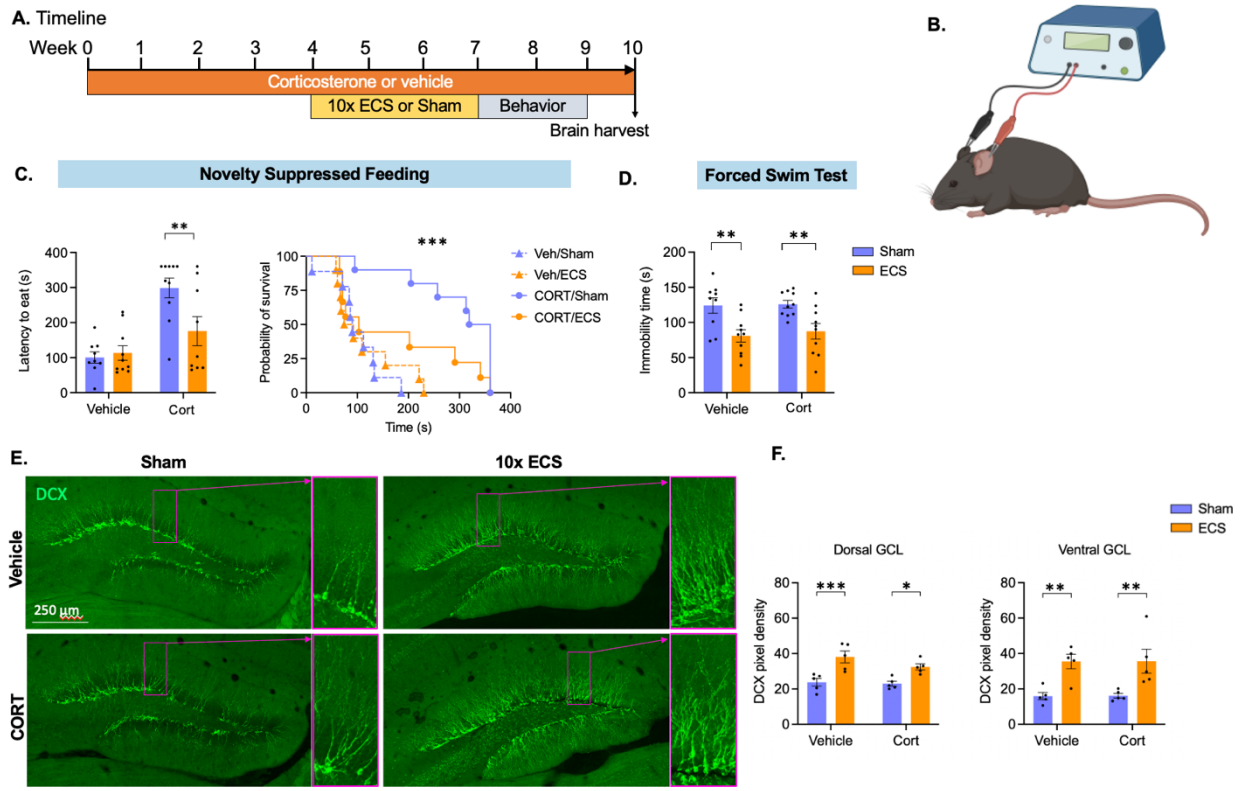

Figure 1. Mouse model of ECS. A) Timeline of the experiment. 10 week-old mice were treated with Vehicle or ~5mg/kg corticosterone (Cort) in drinking water to maintain stress throughout the experiment. After 4 weeks, mice received ECS or Sham treatment every other day for a total of 10 sessions and were tested in paradigms of anxiety-like and depression-like behavior starting 24 hours after the last ECS session. Brains were harvested 1 week after the last behavioral test. **B)** Electroshocks were delivered under isoflurane anesthesia by a Ugo-Basile ECS unit through ear clipped electrodes at 120 Hz, 50 mA for 1s, while Sham mice received anesthesia and ear clip placement, but no electroshock. **C)** In the novelty suppressed feeding test, ECS-treated animals exhibit decreased latency to feed in the Cort group but not in the vehicle group. **D)** In the forced swim test, time spent immobile is reduced after ECS both in the vehicle and Cort groups. **E-F)** Expression of the immature cell marker doublecortin (DCX) is greater in ECS vs Sham subjects. Statistical analyses were performed using Kruskal-Wallis for nonparametric data (C), Mantel-Cox for survival curve (C) and two-way ANOVA for normally distributed data (D, F), (* $p \leq .05$, ** $p \leq .01$, *** $p \leq .001$).

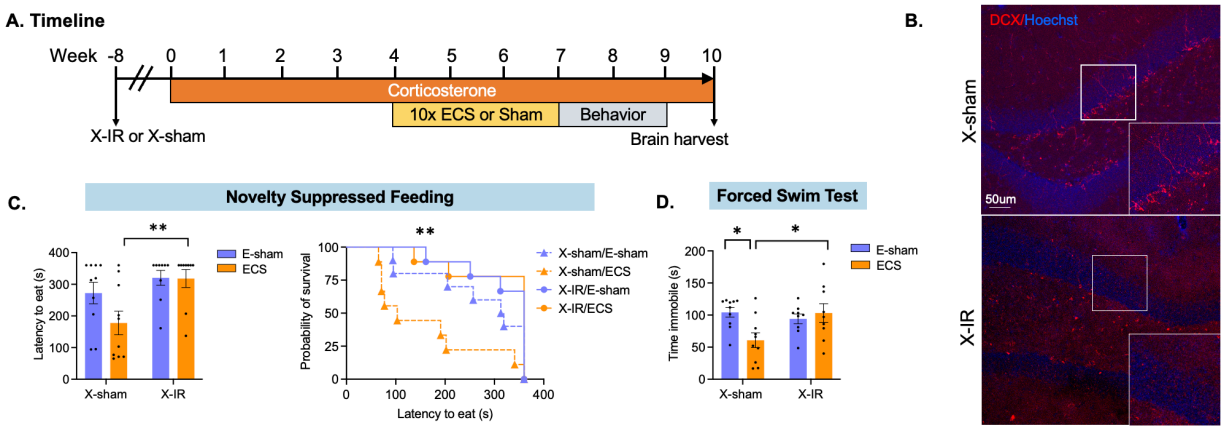

Figure 2. iGCs are required for the behavioral effects of ECS. A) Experimental timeline. Mice received X-irradiation targeting the hippocampus (X-IR) or sham (X-sham). After 8 weeks of recovery, all mice received Cort in drinking water for the duration of the experiment. After 4 weeks, mice received 10 sessions of ECS or Sham (E-sham) and were behaviorally tested in the novelty suppressed feeding test and the forced swim test. **B**) Doublecortin (DCX) immunohistochemistry reveals successful ablation of iGCs in X-IR mice vs. X-sham. **C)** On the NSF test, latency to feed is reduced in ECS-treated mice with intact neurogenesis but not in X-IR mice treated with ECS. **D)** On the FST, X-IR mice receiving ECS do not show decreased immobility time when compared to Sham-treated mice. Statistical analysis was performed using Kruskal-Wallis for nonparametric data (C), Mantel-Cox for survival curve (C) and two-way ANOVA for normally distributed data (D), (* $p \leq .05$, ** $p \leq .01$).

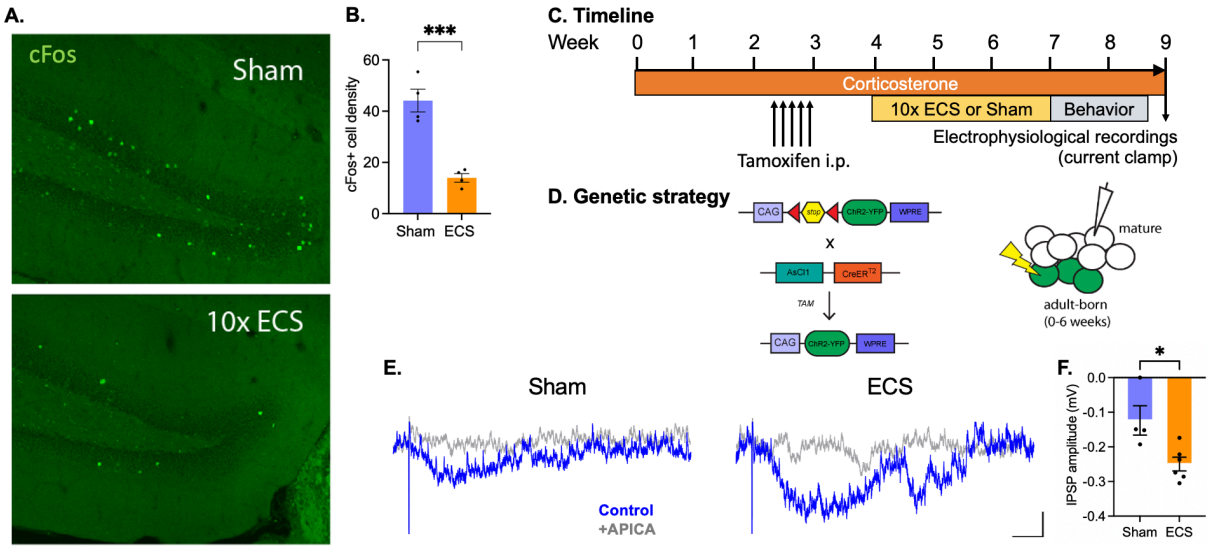

Figure 3. mGluR2 mediates iGC-driven inhibition in mGCs after 10x ECS. A) cFos expression in the granule cell layer of the dentate gyrus following home cage rest is lower in mice that received 10x ECS vs Sham controls (**B**), suggesting that ECS supports a sparser network at rest. **C)** Experimental timeline. Mice received Cort in drinking water for 4 weeks. Tamoxifen was injected 6 weeks to induce expression of ChR2-EYFP in iGCs before performing whole-cell recordings in DG brain slices. Delivery of 10x ECS or Sham occurred one week after tamoxifen-induced Cre recombination. **D)** Breeding strategy and experimental protocol for electrophysiological approach. Nestin-CreER^{T2} mice were crossed with floxed Channelrhodopsin-EYFP (ChR2-EYFP) expressing mice. Optogenetic stimulation of iGCs evoked responses in mGCs. **E)** We optogenetically stimulated 0-6 week-old iGCs to evoke inhibitory postsynaptic potential in mGCs in the presence of 20μM NBQX, 50μM APV, and 20μM bicuculline (blue trace). These inhibitory signals were blocked by bath application of the mGluR2 antagonist APICA (500 μM; grey trace; scale bar = 200 ms, 100 mV). **F)** mGluR2-mediated IPSP had greater negative amplitude after ECS vs Sham in Cort treated mice. (* $p \leq .05$, *** $p \leq .001$).

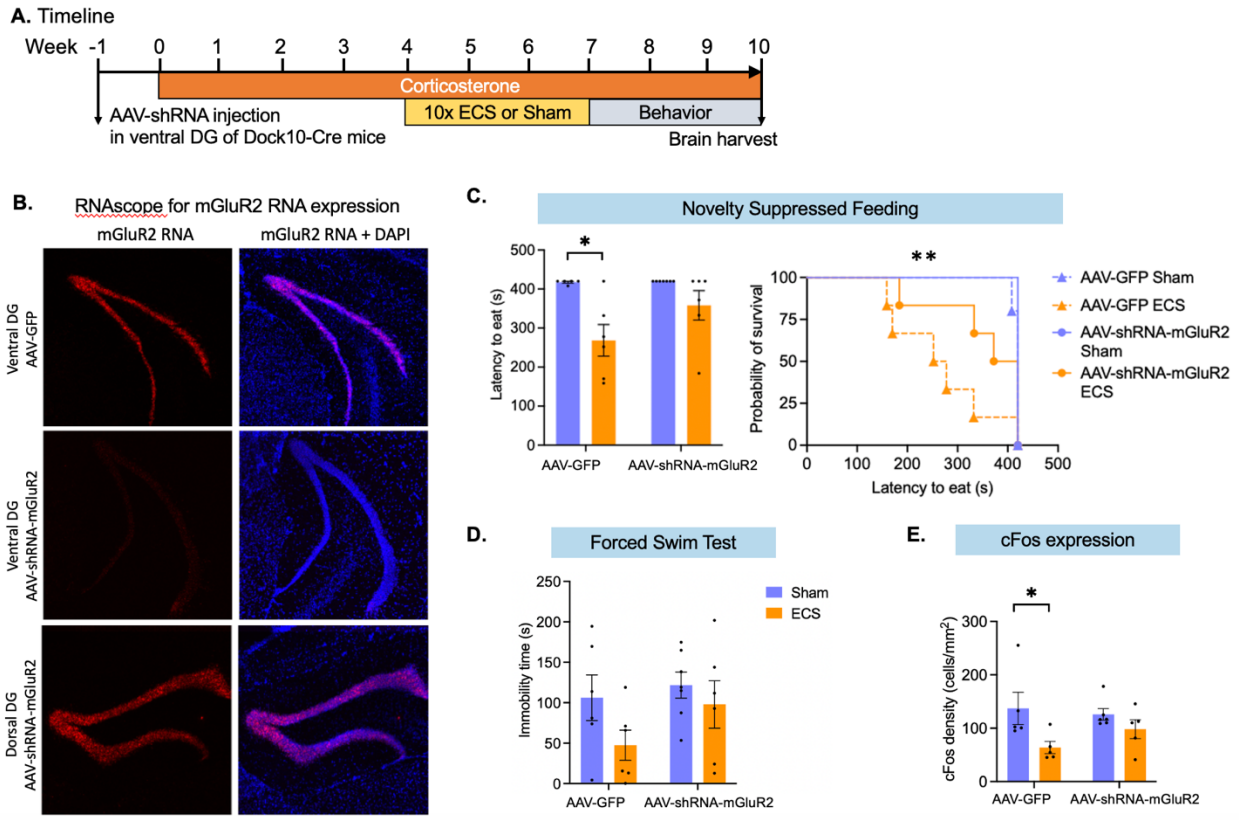

Figure 4. Antidepressant effect of ECS is blunted by mGluR2 knockdown. A) Timeline. Cre-dependent viruses AAV-shRNA-mGluR2 or AAV-GFP control were delivered to the ventral hippocampus of Dock10-Cre mice so that mGluR2 knockdown was limited to ventral DG granule neurons. A week following surgery, mice began Cort treatment in drinking water. After 4 weeks, mice received 10x ECS or Sham, followed by behavioral testing. **B)** In situ hybridization with RNAscope reveals normal mGluR2 RNA expression in the ventral DG of mice injected with the AAV-GFP control virus (top row) and reduced mGluR2 RNA expression in the ventral DG of mice injected with AAV-shRNA-mGluR2. Because injections were localized to the ventral HPC, dorsal HPC expression of mGluR2 is normal in AAV-shRNA-mGluR2 injected tissue. **C)** ECS reduces latency to eat in AAV-GFP controls but not mGluR2 knockdown mice. **D)** No significant behavioral differences are observed in the Forced Swim Test. **E)** ECS significantly reduces cFos density in AAV-GFP controls but not mGluR2 knockdown mice. Statistical analysis was performed using Kruskal-Wallis for nonparametric data (C), Mantel-Cox for survival curve (C) and two-way ANOVA for normally distributed data (D), (* $p \leq .05$, ** $p \leq .01$).

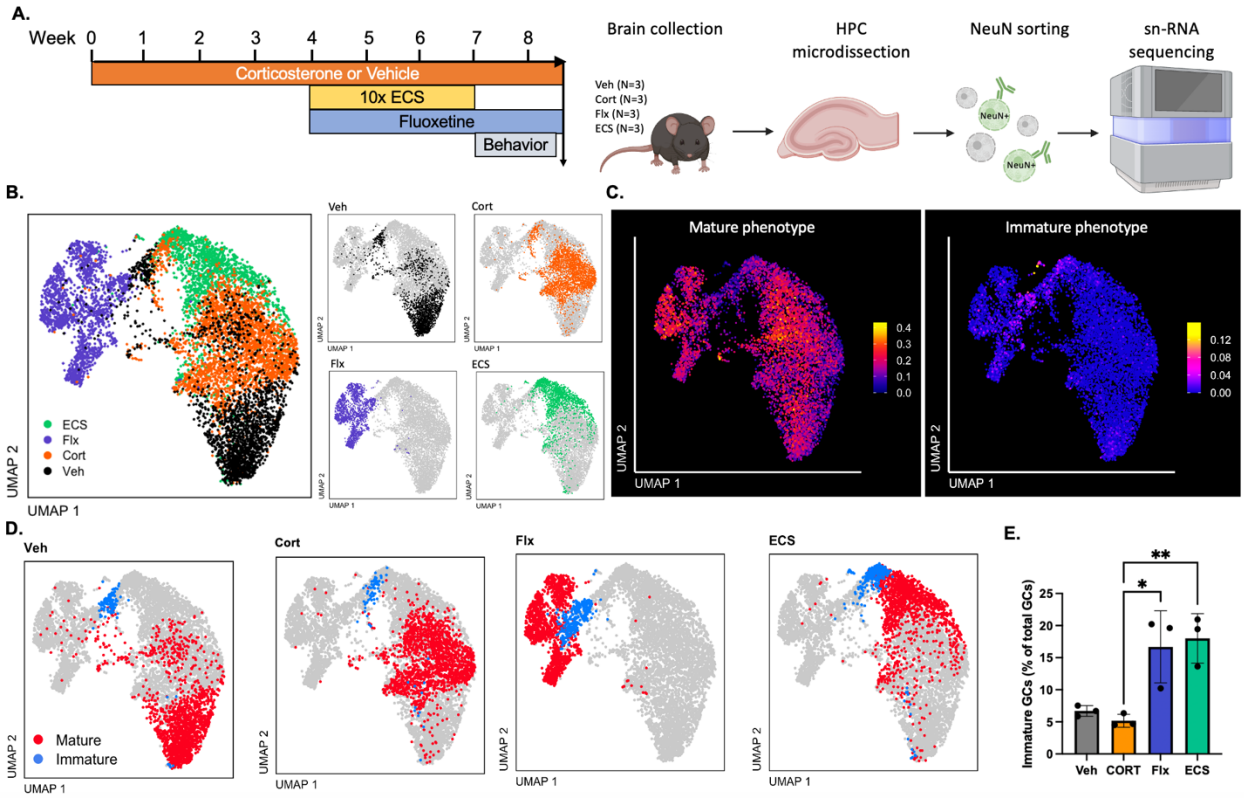

Figure 5. Both ECS and Fluoxetine drive transcriptomic shifts indicating greater neuroplasticity and more prominent immature phenotype among granule neurons. **A**) Single nucleus RNA sequencing was performed on hippocampal nuclei from four treatment groups: vehicle (Veh), corticosterone (Cort), Cort plus fluoxetine (Flx), and Cort plus 10x ECS (N=3 per group). Neuronal nuclei were identified with NeuN antibody followed by cell sorting. UMAP clustering of all neurons revealed a granule neuron population which was used for all subsequent analyses. **B**) UMAP projections of the granule neuron population, labeled by treatment condition. **C**) Genes identified in Hochgerner et al 2018 as those predominantly expressed in either mature or immature cell types were used to produce mature vs immature phenotype module scores. UMAP projections depict granule neurons from all treatment conditions, while color encodes intensity of expression of mature vs immature module scores. **D**) Mature vs immature phenotype module score was used to identify mature vs immature cell clusters. UMAP clustering of mature (red) and immature (blue) nuclei by treatment condition are depicted. **E**) The percent of granule neurons in the immature cell cluster is greater for Flx and ECS treated mice vs Cort alone. Each point represents a single mouse (One-way ANOVA with Tukey posthoc, * $p \leq .05$, ** $p \leq .01$).

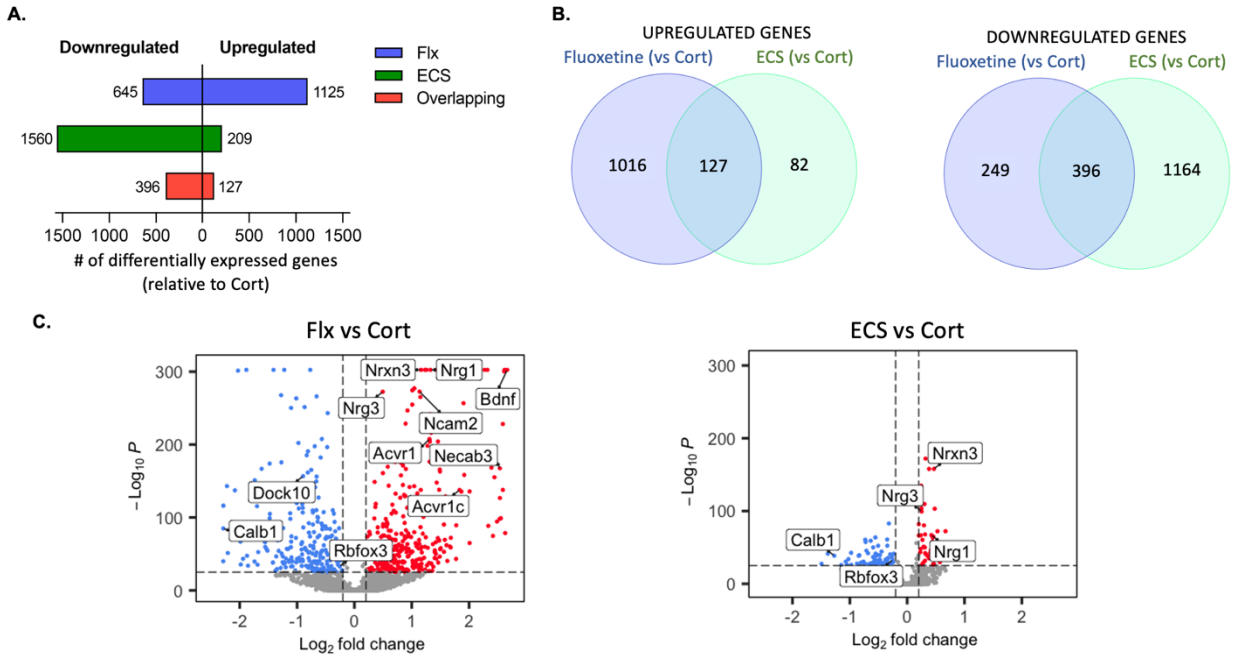

Figure 6. Treatment with fluoxetine induces greater transcriptome upregulation while ECS induces a downward transcriptomic shift. A) Representation of the number of differentially expressed genes (DEGs) that are upregulated (right) vs downregulated (left) for Flx and ECS groups, relative to Cort expression. **B**) Venn diagram depicting overlap of upregulated vs downregulated DEGs in Flx and ECS groups, vs Cort. **C**) Volcano plot depicting expression level (-Log of the p value by Log2 fold change) of DEGs for Flx and ECS groups, vs Cort.

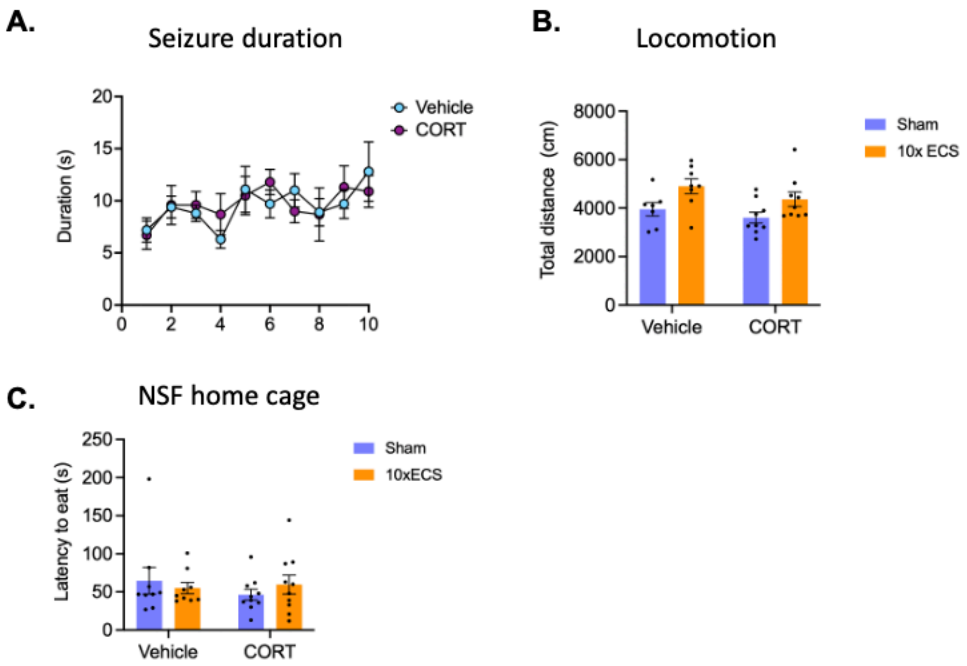

S1. Supplemental figure 1. Additional characterization of the mouse model of ECS. A. Treatment with corticosterone (Cort, purple) vs vehicle (blue) had no impact on duration of seizure. B. Locomotion was measured in an open arena. While two-way ANOVA revealed an effect of ECS treatment ($F(1, 29) = 9.200$; $p = .0051$), post hoc Sidak's test revealed no significant differences in vehicle ($p = .0601$) or Cort treated subjects ($p = .1054$). C. For the NSF, no differences in latency to eat in the home cage were observed.

Acknowledgements.
This work was generously supported by the Hope for Depression Research Foundation (RH), the Jane Coffin Childs Foundation (PN) and the NIMH: R01MH068542 (RH), K08MH122893 (WC), T32MH015144 (AS and PN) and NIA K01 AG054765 (VL). We are grateful to Dr. Joshua Levitz for his insights regarding mGluR2 and to Dr. Marcus Meinhardt for sharing his mGluR2-shRNA vector.

Conflicts of interest.
None of the authors has any conflicts of interest to report.

References.

Al-Harbi, K. S. (2012). Treatment-resistant depression: therapeutic trends, challenges, and future directions. *Patient Prefer Adherence*, *6*, 369-388. https://doi.org/10.2147/ppa.S29716

Anacker, C., Luna, V. M., Stevens, G. S., Millette, A., Shores, R., Jimenez, J. C., Chen, B., & Hen, R. (2018). Hippocampal neurogenesis confers stress resilience by inhibiting the ventral dentate gyrus. *Nature*, *559*(7712), 98-102. https://doi.org/10.1038/s41586-018-0262-4

Bertholomey, M. L., Nagarajan, V., Smith, D. M., & Torregrossa, M. M. (2022). Sex- and age-dependent effects of chronic corticosterone exposure on depressive-like, anxiety-like, and fear-related behavior: Role of amygdala glutamate receptors in the rat. *Front Behav Neurosci*, *16*, 950000. https://doi.org/10.3389/fnbeh.2022.950000

Brunner, J., Ster, J., Van-Weert, S., Andrási, T., Neubrandt, M., Corti, C., Corsi, M., Ferraguti, F., Gerber, U., & Szabadics, J. (2013). Selective silencing of individual dendritic branches by an mGlu2-activated potassium conductance in dentate gyrus granule cells. *J Neurosci*, *33*(17), 7285-7298. https://doi.org/10.1523/jneurosci.4537-12.2013

Butler, A., Hoffman, P., Smibert, P., Papalexi, E., & Satija, R. (2018). Integrating single-cell transcriptomic data across different conditions, technologies, and species. *Nat Biotechnol*, *36*(5), 411-420. https://doi.org/10.1038/nbt.4096

Danielson, N. B., Kaifosh, P., Zaremba, J. D., Lovett-Barron, M., Tsai, J., Denny, C. A., Balough, E. M., Goldberg, A. R., Drew, L. J., Hen, R., Losonczy, A., & Kheirbek, M. A. (2016). Distinct Contribution of Adult-Born Hippocampal Granule Cells to Context Encoding. *Neuron*, *90*(1), 101-112. https://doi.org/10.1016/j.neuron.2016.02.019

Daval, J. L., Nakajima, T., Gleiter, C. H., Post, R. M., & Marangos, P. J. (1989). Mouse brain c-fos mRNA distribution following a single electroconvulsive shock. *J Neurochem*, *52*(6), 1954-1957. https://doi.org/10.1111/j.1471-4159.1989.tb07285.x

David, D. J., Samuels, B. A., Rainer, Q., Wang, J. W., Marsteller, D., Mendez, I., Drew, M., Craig, D. A., Guiard, B. P., Guilloux, J. P., Artymyshyn, R. P., Gardier, A. M., Gerald, C., Antonijevic, I. A., Leonardo, E. D., & Hen, R. (2009). Neurogenesis-dependent and -independent effects of fluoxetine in an animal model of anxiety/depression. *Neuron*, *62*(4), 479-493. https://doi.org/10.1016/j.neuron.2009.04.017

Dieterich, A., Srivastava, P., Sharif, A., Stech, K., Floeder, J., Yohn, S. E., & Samuels, B. A. (2019). Chronic corticosterone administration induces negative valence and impairs positive valence behaviors in mice. *Transl Psychiatry*, *9*(1), 337. https://doi.org/10.1038/s41398-019-0674-4

Dranovsky, A., Picchini, A. M., Moadel, T., Sisti, A. C., Yamada, A., Kimura, S., Leonardo, E. D., & Hen, R. (2011). Experience dictates stem cell fate in the adult hippocampus. *Neuron*, *70*(5), 908-923. https://doi.org/10.1016/j.neuron.2011.05.022

Drew, L. J., Kheirbek, M. A., Luna, V. M., Denny, C. A., Cloidt, M. A., Wu, M. V., Jain, S., Scharfman, H. E., & Hen, R. (2016). Activation of local inhibitory circuits in the dentate gyrus by adult-born neurons. *Hippocampus*, *26*(6), 763-778. https://doi.org/10.1002/hipo.22557

Gonzalez, J. C., Epps, S. A., Markwardt, S. J., Wadiche, J. I., & Overstreet-Wadiche, L. (2018). Constitutive and Synaptic Activation of GIRK Channels Differentiates Mature and Newborn Dentate Granule Cells. *J Neurosci*, *38*(29), 6513-6526. https://doi.org/10.1523/jneurosci.0674-18.2018

Hagihara, H., Ohira, K., & Miyakawa, T. (2019). Transcriptomic evidence for immaturity induced by antidepressant fluoxetine in the hippocampus and prefrontal cortex. *Neuropsychopharmacol Rep*, *39*(2), 78-89. https://doi.org/10.1002/npr2.12048

Henningsen, K., Woldbye, D. P., & Wiborg, O. (2013). Electroconvulsive stimulation reverses anhedonia and cognitive impairments in rats exposed to chronic mild stress. *Eur Neuropsychopharmacol*, *23*(12), 1789-1794. https://doi.org/10.1016/j.euroneuro.2013.03.011

Hill, A. S., Sahay, A., & Hen, R. (2015). Increasing Adult Hippocampal Neurogenesis is Sufficient to Reduce Anxiety and Depression-Like Behaviors. *Neuropsychopharmacology*, *40*(10), 2368-2378. https://doi.org/10.1038/npp.2015.85

Hochgerner, H., Zeisel, A., Lönnerberg, P., & Linnarsson, S. (2018). Conserved properties of dentate gyrus neurogenesis across postnatal development revealed by single-cell RNA sequencing. *Nat Neurosci*, *21*(2), 290-299. https://doi.org/10.1038/s41593-017-0056-2

Husain, M. M., Rush, A. J., Fink, M., Knapp, R., Petrides, G., Rummans, T., Biggs, M. M., O'Connor, K., Rasmussen, K., Litle, M., Zhao, W., Bernstein, H. J., Smith, G., Mueller, M., McClintock, S. M., Bailine, S. H., & Kellner, C. H. (2004). Speed of response and remission in major depressive disorder with acute electroconvulsive therapy (ECT): a Consortium for Research in ECT (CORE) report. *J Clin Psychiatry*, *65*(4), 485-491. https://doi.org/10.4088/jcp.v65n0406

Ittasakul, P., Vora-Arporn, S., Waleeprakhon, P., & Tor, P. C. (2020). Number of Electroconvulsive Therapy Sessions required for Thai Psychiatric Patients: a Retrospective Study. *Neuropsychiatr Dis Treat*, *16*, 673-679. https://doi.org/10.2147/ndt.S244031

Kheirbek, M. A., Drew, L. J., Burghardt, N. S., Costantini, D. O., Tannenholz, L., Ahmari, S. E., Zeng, H., Fenton, A. A., & Hen, R. (2013). Differential control of learning and anxiety along the dorsoventral axis of the dentate gyrus. *Neuron*, *77*(5), 955-968. https://doi.org/10.1016/j.neuron.2012.12.038

Kobayashi, K., Ikeda, Y., Sakai, A., Yamasaki, N., Haneda, E., Miyakawa, T., & Suzuki, H. (2010). Reversal of hippocampal neuronal maturation by serotonergic antidepressants. *Proc Natl Acad Sci U S A*, *107*(18), 8434-8439. https://doi.org/10.1073/pnas.0912690107

Kohara, K., Pignatelli, M., Rivest, A. J., Jung, H. Y., Kitamura, T., Suh, J., Frank, D., Kajikawa, K., Mise, N., Obata, Y., Wickersham, I. R., & Tonegawa, S. (2014). Cell type-specific genetic and optogenetic tools reveal hippocampal CA2 circuits. *Nat Neurosci*, *17*(2), 269-279. https://doi.org/10.1038/nn.3614

Li, H., Tamura, R., Hayashi, D., Asai, H., Koga, J., Ando, S., Yokota, S., Kaneko, J., Sakurai, K., Sumiyoshi, A., Yamamoto, T., Hikishima, K., Tanaka, K. Z., McHugh, T. J., & Hisatsune, T. (2024). Silencing dentate newborn neurons alters excitatory/inhibitory balance and impairs behavioral inhibition and flexibility. *Sci Adv*, *10*(2), eadk4741. https://doi.org/10.1126/sciadv.adk4741

Linden, A. M., Greene, S. J., Bergeron, M., & Schoepp, D. D. (2004). Anxiolytic activity of the MGLU2/3 receptor agonist LY354740 on the elevated plus maze is associated with the suppression of stress-induced c-Fos in the hippocampus and increases in c-Fos induction in several other stress-sensitive brain regions. *Neuropsychopharmacology*, *29*(3), 502-513. https://doi.org/10.1038/sj.npp.1300321

Loef, D., Tendolkar, I., van Eijndhoven, P. F. P., Hoozemans, J. J. M., Oudega, M. L., Rozemuller, A. J. M., Lucassen, P. J., Dols, A., & Dijkstra, A. A. (2023). Electroconvulsive therapy is associated with increased immunoreactivity of neuroplasticity markers in the hippocampus of depressed patients. *Transl Psychiatry*, *13*(1), 355. https://doi.org/10.1038/s41398-023-02658-1

Luna, V. M., Anacker, C., Burghardt, N. S., Khandaker, H., Andreu, V., Millette, A., Leary, P., Ravenelle, R., Jimenez, J. C., Mastrodonato, A., Denny, C. A., Fenton, A. A., Scharfman, H. E., & Hen, R. (2019). Adult-born hippocampal neurons bidirectionally modulate entorhinal inputs into the dentate gyrus. *Science*, *364*(6440), 578-583. https://doi.org/10.1126/science.aat8789

Ma, J., Hu, Z., Yue, H., Luo, Y., Wang, C., Wu, X., Gu, Y., & Wang, L. (2023). GRM2 Regulates Functional Integration of Adult-Born DGCs by Paradoxically Modulating MEK/ERK1/2 Pathway. *J Neurosci*, *43*(16), 2822-2836. https://doi.org/10.1523/jneurosci.1886-22.2023

McHugh, S. B., Lopes-Dos-Santos, V., Gava, G. P., Hartwich, K., Tam, S. K. E., Bannerman, D. M., & Dupret, D. (2022). Adult-born dentate granule cells promote hippocampal population sparsity. *Nat Neurosci*, *25*(11), 1481-1491. https://doi.org/10.1038/s41593-022-01176-5

Meyers, K. T., Damphousse, C. C., Ozols, A. B., Campbell, J. M., Newbern, J. M., Hu, C., Marrone, D. F., & Gallitano, A. L. (2023). Serial electroconvulsive Seizure alters dendritic complexity and promotes cellular proliferation in the mouse dentate gyrus; a role for Egr3. *Brain Stimul*, *16*(3), 889-900. https://doi.org/10.1016/j.brs.2023.04.022

Munguba, H., Gutzeit, V. A., Srivastava, I., Kristt, M., Singh, A., Vijay, A., Arefin, A., Thukral, S., Broichhagen, J., Stujenske, J. M., Liston, C., & Levitz, J. (2024). Projection-Targeted Photopharmacology Reveals Distinct Anxiolytic Roles for Presynaptic mGluR2 in Prefrontal- and Insula-Amygdala Synapses. *bioRxiv*. https://doi.org/10.1101/2024.01.15.575699

Nguyen, P. T., Dorman, L. C., Pan, S., Vainchtein, I. D., Han, R. T., Nakao-Inoue, H., Taloma, S. E., Barron, J. J., Molofsky, A. B., Kheirbek, M. A., & Molofsky, A. V. (2020). Microglial Remodeling of the Extracellular Matrix Promotes Synapse Plasticity. *Cell*, *182*(2), 388-403.e315. https://doi.org/10.1016/j.cell.2020.05.050

Nuninga, J. O., Mandl, R. C. W., Boks, M. P., Bakker, S., Somers, M., Heringa, S. M., Nieuwdorp, W., Hoogduin, H., Kahn, R. S., Luijten, P., & Sommer, I. E. C. (2020). Volume increase in the dentate gyrus after electroconvulsive therapy in depressed patients as measured with 7T. *Mol Psychiatry*, *25*(7), 1559-1568. https://doi.org/10.1038/s41380-019-0392-6

Rimmerman, N., Verdiger, H., Goldenberg, H., Naggan, L., Robinson, E., Kozela, E., Gelb, S., Reshef, R., Ryan, K. M., Ayoun, L., Refaeli, R., Ashkenazi, E., Schottlender, N., Ben Hemo-Cohen, L., Pienica, C., Aharonian, M., Dinur, E., Lazar, K., McLoughlin, D. M., . . . Yirmiya, R. (2022). Microglia and their LAG3 checkpoint underlie the antidepressant and

neurogenesis-enhancing effects of electroconvulsive stimulation. *Mol Psychiatry*, *27*(2), 1120-1135. https://doi.org/10.1038/s41380-021-01338-0

Rush, A. J., South, C., Jha, M. K., Jain, S. B., & Trivedi, M. H. (2020). What to Expect When Switching to a Second Antidepressant Medication Following an Ineffective Initial SSRI: A Report From the Randomized Clinical STAR*D Study. *J Clin Psychiatry*, *81*(5). https://doi.org/10.4088/JCP.19m12949

Sahay, A., Scobie, K. N., Hill, A. S., O'Carroll, C. M., Kheirbek, M. A., Burghardt, N. S., Fenton, A. A., Dranovsky, A., & Hen, R. (2011). Increasing adult hippocampal neurogenesis is sufficient to improve pattern separation. *Nature*, *472*(7344), 466-470. https://doi.org/10.1038/nature09817

Samuels, B. A., & Hen, R. (2011). Novelty-Suppressed Feeding in the Mouse. *Neuromethods*, *63*, 14.

Santarelli, L., Saxe, M., Gross, C., Surget, A., Battaglia, F., Dulawa, S., Weisstaub, N., Lee, J., Duman, R., Arancio, O., Belzung, C., & Hen, R. (2003). Requirement of hippocampal neurogenesis for the behavioral effects of antidepressants. *Science*, *301*(5634), 805-809. https://doi.org/10.1126/science.1083328

Satija, R., Farrell, J. A., Gennert, D., Schier, A. F., & Regev, A. (2015). Spatial reconstruction of single-cell gene expression data. *Nat Biotechnol*, *33*(5), 495-502. https://doi.org/10.1038/nbt.3192

Schloesser, R. J., Orvoen, S., Jimenez, D. V., Hardy, N. F., Maynard, K. R., Sukumar, M., Manji, H. K., Gardier, A. M., David, D. J., & Martinowich, K. (2015). Antidepressant-like Effects of Electroconvulsive Seizures Require Adult Neurogenesis in a Neuroendocrine Model of Depression. *Brain Stimul*, *8*(5), 862-867. https://doi.org/10.1016/j.brs.2015.05.011

Segi-Nishida, E., Warner-Schmidt, J. L., & Duman, R. S. (2008). Electroconvulsive seizure and VEGF increase the proliferation of neural stem-like cells in rat hippocampus. *Proc Natl Acad Sci U S A*, *105*(32), 11352-11357. https://doi.org/10.1073/pnas.0710858105

Suzuki, M., & Masuda, Y. (1999). Effect of repeated electroconvulsive shock treatment on a depression model, mouse forced swimming. *Tohoku J Exp Med*, *189*(1), 83-86. https://doi.org/10.1620/tjem.189.83

Tuncdemir, S. N., Grosmark, A. D., Chung, H., Luna, V. M., Lacefield, C. O., Losonczy, A., & Hen, R. (2023). Adult-born granule cells facilitate remapping of spatial and non-spatial representations in the dentate gyrus. *Neuron*, *111*(24), 4024-4039.e4027. https://doi.org/10.1016/j.neuron.2023.09.016

Ueno, M., Sugimoto, M., Ohtsubo, K., Sakai, N., Endo, A., Shikano, K., Imoto, Y., & Segi-Nishida, E. (2019). The effect of electroconvulsive seizure on survival, neuronal differentiation, and expression of the maturation marker in the adult mouse hippocampus. *J Neurochem*, *149*(4), 488-498. https://doi.org/10.1111/jnc.14691

Yoshimizu, T., Shimazaki, T., Ito, A., & Chaki, S. (2006). An mGluR2/3 antagonist, MGS0039, exerts antidepressant and anxiolytic effects in behavioral models in rats. *Psychopharmacology (Berl)*, *186*(4), 587-593. https://doi.org/10.1007/s00213-006-0390-7

Zhao, C., Warner-Schmidt, J., Duman, R. S., & Gage, F. H. (2012). Electroconvulsive seizure promotes spine maturation in newborn dentate granule cells in adult rat. *Dev Neurobiol*, *72*(6), 937-942. https://doi.org/10.1002/dneu.20986

Zhdanava, M., Pilon, D., Ghelerter, I., Chow, W., Joshi, K., Lefebvre, P., & Sheehan, J. J. (2021). The Prevalence and National Burden of Treatment-Resistant Depression and Major Depressive Disorder in the United States. *J Clin Psychiatry*, *82*(2). https://doi.org/10.4088/JCP.20m13699